ACS Macro Letters

Letter

pubs.acs.org/macroletters

Shear Banding in Telechelic Associative Polymers by Molecular Dynamics

J. Castillo-Tejas,*[,†] S. Carro,[†] and O. Manero*[,‡]

[†]Facultad de Ciencias Básicas, Ingeniería y Tecnología, Universidad Autónoma de Tlaxcala, Apizaco, Tlaxcala 90300, México

[‡]Instituto de Investigaciones en Materiales, Universidad Nacional Autónoma de México, México, D.F., 04510, México

ABSTRACT: Results on the shear flow of telechelic associative polymers using nonequilibrium molecular dynamics (NEMD) are presented. The particle stream velocities can be calculated from the peculiar velocities and the imposed velocity profile using a novel approach. The constitutive relationship *stress–shear rate* becomes nonmonotonic when the interaction force between hydrophobic sites is increased. This condition induces a steady banding flow, which arises under transient conditions as a local instability originated from the breakage of micellar aggregates, thus promoting the migration of these aggregates to regions of low velocity gradients. Here, for the first time, NEMD simulations predict the banding flow of associative polymers.

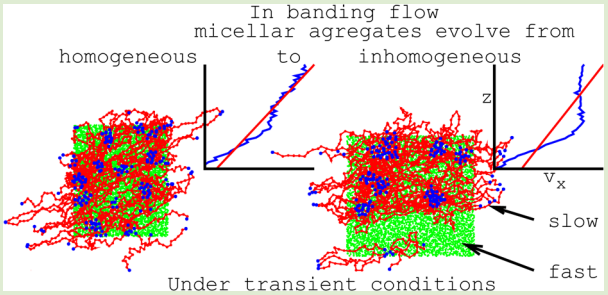

The flow of complex fluids displays interesting rheological manifestations, such as the appearance of bands of different shear rate along the velocity gradient direction or, in some occasions, along the vorticity direction. Gradient bands are associated with extreme shear thinning, such as a stress plateau arising in the constitutive *stress–shear rate curve*. The extremes of the plateau are located at critical shear rates, representing two velocity gradient regions in the flow field coexisting with the same steady stress. In each band, the velocity gradient is essentially constant. The objective of the present work is focused on the understanding of the molecular processes that give rise to gradient-banded flow observed in telechelic associative polymers, which are important because of their industrial applications (paints, coating, water treatment, enhanced oil recovery).

Generally speaking, banded flow is attributed to changes in the microscopic organization of the fluid induced by the shear rate, implying conformational changes such as orientation and disentanglement of aggregates.[1] Shear banding flow has been observed in micellar solutions[2−6] and associative polymers.[7,8] In the case of micellar solutions, banding flow has been related to a constitutive instability, in which for increasing shear rates a nonmonotonic stress region arises with a negative slope. For telechelic associative polymers, Sprakel et al.[8] pointed out that banding flow results from the effect of shear rate on the lifetime of the bridges between aggregates, an important aspect which is analyzed in detail in this letter.

A relevant study on the origin of banded flow has been set out by Marrucci and Grizzuti.[9] Using the Doi and Edwards model[10] they estimate the free energy as a function of the shear rate, identifying the inflection point in the free energy associated with an instability or nonhomogeneities in the system, which persist up to the occurrence of orientation relaxation. This analysis suggests the possibility that instabilities, or "deformational phase separations", arise in the course of stress relaxation experiments. Further studies proceeded to investigate the molecular origin of banded flow in entangled melts.[11,12] Cao and Likhtman[13] use molecular dynamics to simulate the simple shear flow of entangled melts, represented by bead–spring models. A nonmonotonic constitutive flow curve is predicted. Under transient conditions within the instability region, linear velocity profiles are simulated before stress overshoot. Past the stress peak, the velocity profile becomes nonlinear, and banded flow is induced. In addition, in entangled melts, Mohagheghi and Khomani[11] use *Dissipative Particle Dynamics* to simulate a nonmonotonic relationship of shear stress–shear rate under simple shear flow. In transient flow, a stress maximum is observed upon inception of shear flow, related to the onset of local instabilities, which lead to banded flow. It is predicted to occur when the conformational relaxation of the chains in transient flow takes place in a longer time scale than that of stress relaxation.

Banded flow studies on entangled melts[11−13] and associative polymers[8] reveal that the induction of banded flow is associated with the existence of a nonmonotonic flow curve, the presence of local instabilities during stress relaxation, and the lifetime of the associations among micellar aggregates. Here, we apply the concepts set out by Marrucci and Grizzuti to shed light on the molecular origin of banded flow in associative polymers. For this sake, a simple shear flow is simulated using the NEMD technique within a *NVT* ensemble. Under steady flow, the constitutive stress–shear rate curve is computed, in addition to final configurations and velocity profiles along the gradient

Received: November 28, 2016
Accepted: February 8, 2017
Published: February 10, 2017

DOI: 10.1021/acsmacrolett.6b00906
ACS Macro Lett. 2017, 6, 190−193

direction. Under transient flow, predictions of shear stress, velocity profiles ($v_x(z)$), distance between hydrophobic sites ($f(r)$), density profiles ($\rho(z)$), and coordination numbers (n_c) are included.

The constitutive curve is made nondimensional using the main relaxation time of the system (λ = 2000) and the elastic modulus (G_0 = 0.0453), which can be obtained from rheometric data. Figure 1 displays the constitutive curve within

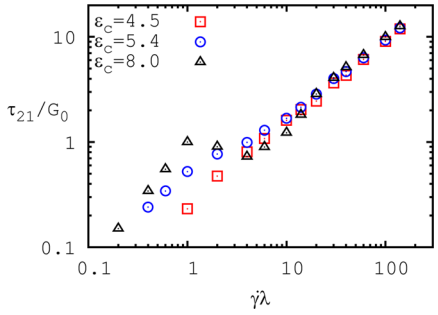

Figure 1. Variation of shear stress (τ_{21}/G_0) as a function of shear rate ($\dot{\gamma}\lambda$) for ε_c = 4.5, 5.4, and 8.0.

the shear rate range of $0.2 \leq \dot{\gamma}\lambda \leq 140.0$ for various values of the interaction parameter between hydrophobic sites (ε_c), and in Figure 2 the two-dimensional final configurations for ε_c = 8.0

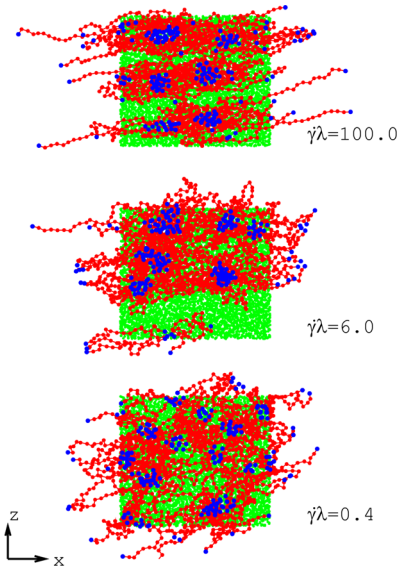

Figure 2. Two-dimensional steady-state configuration of the solution for ε_c = 8.0, where the green, red, and blue particles correspond to solvent, chain, and hydrophobic sites, respectively.

and $\dot{\gamma}\lambda$ of 0.4, 6.0, and 100.0 are shown. Results indicate that the interaction parameter determines the degree of association between the hydrophobic sites affecting the constitutive curve. Upon increasing ε_c the shear stress increases, exhibiting three flow regions. At low shear rates, the stress is linear with the shear rate (Newtonian region), which ends around $\dot{\gamma}\lambda$ = 0.6. Within $1.0 \leq \dot{\gamma}\lambda \leq 10.0$ the shear stress is monotonic (ε_c of 4.5 and 5.4) and nonmonotonic (ε_c = 8.0 where the slope is negative ($d\tau_{21}/d\dot{\gamma} < 0$)) exhibiting a pronounced shear thinning, corresponding presumably to the banded flow condition. For $\dot{\gamma}\lambda \geq 14.0$ the stress increases linearly with shear rate again, with a slope independent of the interaction parameter. With respect to molecular configurations (see Figure 2), for the first region ($\dot{\gamma}\lambda$ = 0.4) aggregates forming micellar flowers are distributed randomly in the flow domain, with bridges between the flowers and dangling chains near the edges of the simulation region. At $\dot{\gamma}\lambda$ = 6.0, the nuclei of the flowers aggregate, gathering together in the upper section of the simulation region coexisting with solvent particles in the lower section of the flow domain. At $\dot{\gamma}\lambda$ = 100.0, aggregates of flower nuclei are observed, remarkably ordered within three layers equally distributed along the gradient direction. Note that this configuration will be related with modifications and oscillations of the initial velocity gradient as shown in Figure 3a.

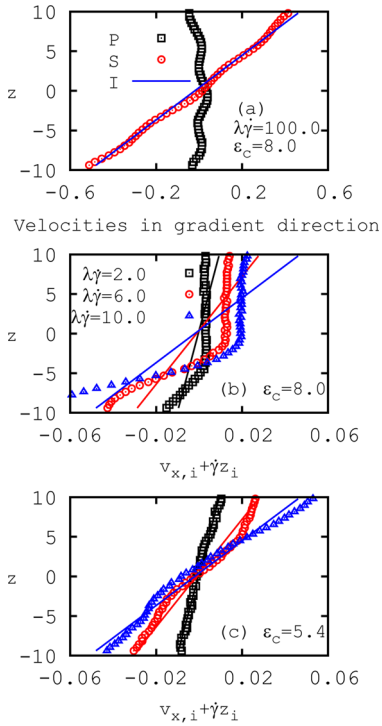

Figure 3. (a) Characteristic flow velocities along the gradient direction (peculiar (P), black squares; imposed (I), blue line and stream (S), red circles). (b, c) Imposed and stream velocity profiles at shear rates corresponding to the nonmonotonic flow region, for values of the interaction parameter ε_c of 8.0 and 5.4.

In solving the equations of motion, the peculiar velocity of a particle in flow direction ($v_{x,i}$) is known, and hence its stream velocity is equal to the peculiar one plus the imposed velocity profile ($\dot{\gamma}z_i$). Although the SLLOD dynamics imposes this linear velocity profile ($\dot{\gamma}z_i$), the bulk flow develops a stream velocity ($v_{xi} + \dot{\gamma}z_i$) consistent with the imposed flow, particle interactions, and local density fluctuations. In Figure 3 results are shown on: (a) peculiar, stream, and imposed velocities and (b and c) stream velocity profiles ($v_{x,i} + \dot{\gamma}z_i$) for ε_c of 8.0 and 5.4, respectively, at $\dot{\gamma}\lambda$ of 2.0, 6.0, and 10.0. These shear rates correspond to the second flow region (nonmonotonic region) of the constitutive curve where banded flow arises.

Molecular dynamics simulations of entangled melts by Cao and Likhtman[13] include SLLOD dynamics to calculate the constitutive curve and *Dissipative Particle Dynamics* to obtain stream velocity profiles under shear flow conditions. Here, using a novel approach, we demonstrate that it is possible to obtain stream velocities in shear flow solely with SLLOD dynamics. For ε_c = 8.0 and $\dot{\gamma}\lambda$ = 100.0 (see Figure 3a), flow

DOI: 10.1021/acsmacrolett.6b00906
ACS Macro Lett. 2017, 6, 190−193

corresponds to the high shear-rate region, developing a *linear stream velocity profile* ($v_{x,i} + \dot{\gamma} z_i$). Notice that the peculiar velocity ($v_{x,i}$) oscillates around zero, conserving momentum along the flow direction, which reveals that the solution is consistent with the flow developed by the SLLOD dynamics. This behavior of the peculiar velocity is the same within the entire interval of shear rates.

For ε_c equal to 4.5 (not shown) and 5.4 (Figure 3c), stream velocity profiles oscillate around the imposed velocity profile, but the fluid is still homogeneous. However, when ε_c = 8.0 (Figure 3b), the stream velocity ceases to oscillate and exhibits two regions of different velocity profiles, a fast flow in the lower section of the simulation domain, and a slow one, almost a plug profile, in the upper section of the flow domain. These predictions demonstrate the existence of banded flow within shear rates corresponding to the nonmonotonic region of the constitutive curve. Final conformations at $\dot{\gamma}\lambda$ = 6.0 (see Figure 2) indicate that under banded flow conditions polymer molecules and aggregates appear in the region of slow flow, while the solvent particles locate in the fast flow region. This result evidences the induction of a nonequilibrium phase separation similar to that observed in complex fluids undergoing spinodal decomposition.

In Figure 4 the variation of the shear stress, molecular conformation, and stream velocity with strain, under banded

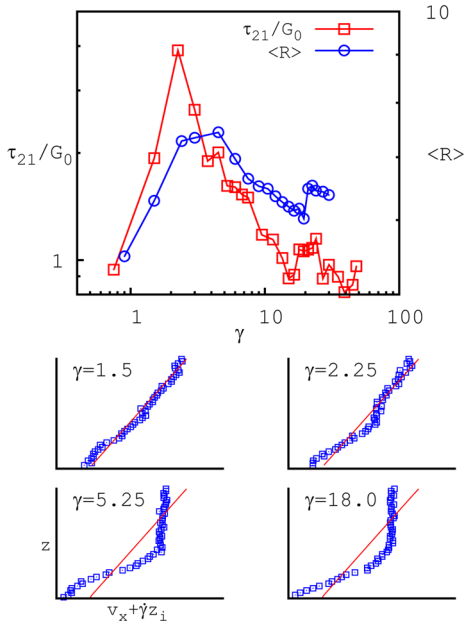

Figure 4. Shear stress, end-to-end distance as a function of strain, and stream velocity profiles under transient flow for ε_c = 8.0 and $\dot{\gamma}\lambda$ = 6.0 are shown.

flow, are displayed (ε_c = 8.0, $\dot{\gamma}\lambda$ = 6.0). Initially, the stress increases linearly with strain up to a maximum of 3.88 at $\gamma \sim$ 2.2. Thereafter, stress relaxation with slower rate to achieve the steady state is observed. This relaxation behavior is consistent with that observed in polymer melts.[11,13] The end-to-end distance ($\langle R \rangle$) under transient flow exhibits a similar behavior to that of the stress. However, past the stress maximum, molecules continue deforming before relaxing; this process occurs within the same time scale. Velocity profiles are linear prior to the stress peak (γ = 1.5), but just at the maximum (γ = 2.2), instability appears in the lower section of the domain. At a strain of 5.25, the instability increases with sections of high shear rates up to a strain of 18.0 where two regions of different flow conditions (a fast and a slow one) appear, which is the signature of banded flow.

Results evidence that banded flow is associated with a local instability in the velocity profile, which increases during stress relaxation. To further elucidate the causes of this instability, in Figure 5 results are shown on: (a) distance between

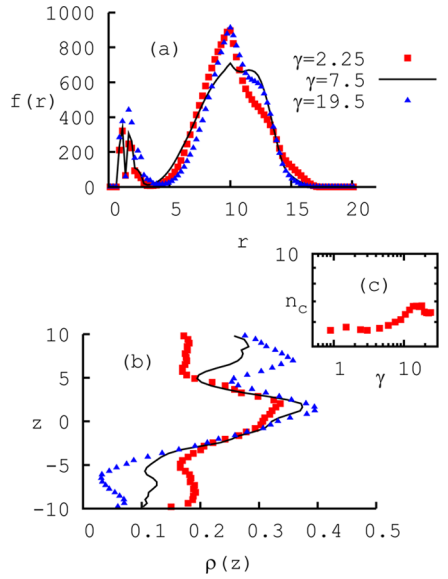

Figure 5. (a) Distance between hydrophobic sites (in terms of frequencies, $f(r)$), (b) density profiles of chain segments ($\rho(z)$), and (c) coordination number (n_c) in the transient regime for ε_c = 8.0 and $\dot{\gamma}\lambda$ = 6.0.

hydrophobic sites ($f(r)$), (b) density profiles ($\rho(z)$) of chain segments along the gradient direction, and (c) coordination number (n_c). The distance between hydrophobic sites (in terms of frequencies) exhibits three peaks, at 1σ, 1.7σ, and 10.0σ (see Figure 5a), respectively, of which the first two peaks are associated with the nuclei of micellar flowers,[15] while the third peak should be related with the connecting bridges of the flowers. During the relaxation period of the stress and molecular conformation, the value of the third peak of $f(r)$ diminishes progressively to ~708.0 corresponding to a strain of 7.5 and thereafter increases up to that of the initial value of the relaxation process. This behavior reveals kinetics of connection−disconnection among the micellar flowers along the nonmonotonic region of the constitutive curve. In Figure 5c, for $\gamma \leq$ 6.0, the coordination number remains constant, around ~5.6. Since n_c is related with the number of neighbors in the first solvation layer, the number of hydrophobic sites that conform the flowers nuclei is kept constant during the time of the decrease in $f(r)$, and thereafter it increases. Therefore, it is evident that flowers disconnect within an ongoing kinetic process. Figure 5b depicts that in the stress maximum (γ = 2.25) chain segments distribute heterogeneously along the density gradient since the central symmetry line corresponds to a density of ~0.3, which diminishes to ~0.2 in the upper and lower regions of the simulation domain. During stress relaxation (γ = 7.5), the number of chains in the lower section diminishes, increasing along the symmetry line and the upper section of the domain, such that within these regions molecular aggregates gather in two layers.

DOI: 10.1021/acsmacrolett.6b00906
ACS Macro Lett. 2017, 6, 190−193

Under a steady state, the presence of banded flow depends on the interaction force between hydrophobic sites and occurs within the nonmonotonic region of the constitutive curve, but the origin of such flow occurs under transient conditions. In this regime, banded flow arises as a local instability during stress relaxation, originated by a disconnection process among the micellar aggregates, which promotes the migration of aggregates and chains to lower velocity gradients. As the aggregates gather in a confined region of the flow domain, the reconnection process sets in, as the hydrophobic groups reform the micellar flower nuclei. As a global conclusion, in this work we demonstrate that nonequilibrium molecular dynamics simulations can predict the banding flow in telechelic associative polymers.

METHODS

The solution is formed by linear chains immersed in solvent particles at a reduced density and temperature of 1.0 and 1.5, respectively. Each molecule is composed of 20 joined segments represented by a bead−spring model.[14] The system amounts to 8000 total sites, of which 2000 sites correspond to molecular chains, such that the concentration per site (c) is 0.25. The intermolecular potentials present in the associative polymer solution comprise a Lennard-Jones (L-J) potential[15] for attraction and repulsive interactions among the solution components, an attractive FENE potential, which together with the repulsive L-J potential built the links between molecular segments, and finally, an attractive potential to represent the hydrophobic site interactions (HS) given by the following expression[16]

$$U(r_{ij}) = -\frac{\varepsilon_c}{r_{ij}}\left[1 - \left(\frac{r_{ij}}{r_c}\right)^2\right]^2 \quad (1)$$

r_{ij} is the distance between particles i and j; r_c (= 2.5σ, where σ is molecular diameter) is the critical distance of HS interactions; and ε_c is the energy parameter associated with the interaction or association force between hydrophobic sites. These sites are located at the extremes of the chain to reproduce the behavior of telechelic polymers.[15] The concentration per site of the solution (c = 0.25) corresponds to the end of the semidiluted regime, which allows the association of two hydrophobic sites with a third hydrophobic site at ε_c = 5.4.[15] At this concentration and energy parameter between HS, the molecular configuration displays connected "flowers". To elucidate the effect of entanglements between aggregates on rheological behavior, nonequilibrium simulations are performed at three different values of ε_c (4.5, 5.4, and 8).

The shear flow is generated by using SLLOD[17] dynamics coupled with periodic boundary conditions of Lee and Edwards.[18] Within this dynamics, a velocity profile is imposed ($\mathbf{r}_i \cdot \nabla \mathbf{v}$) to the particles, which themselves develop a peculiar velocity after resting the x-component of the momentum flux along the gradient direction ($\mathbf{v}_i \cdot \nabla \mathbf{v}$), as shown in the following equations of motion

$$\frac{d\mathbf{r}_i}{dt} = \mathbf{v}_i + \mathbf{r}_i \cdot \nabla \mathbf{v} \quad (2)$$

$$\frac{d\mathbf{v}_i}{dt} = \frac{\mathbf{F}_i}{m_i} - \mathbf{v}_i \cdot \nabla \mathbf{v} - V_\xi \mathbf{v}_i \quad (3)$$

$\mathbf{r}_i$, $\mathbf{v}_i$, and $\mathbf{F}_i$ are the position, peculiar velocity, and force vectors associated with a particle i, respectively. The flow direction is x, and z is the gradient direction, such that $\nabla \mathbf{v} = \dot{\gamma}\mathbf{ki}$ and $\dot{\gamma}$ is the shear rate. Simulations are carried out at constant temperature using a Nosé−Hoover thermostat,[19] where V_ξ is the dynamics variable of the thermostat. Under this simulation scheme, it is demonstrated that a nonmonotonic behavior of the constitutive curve and stream velocity profiles can be resolved. All results of the simulations are expressed in reduced units.

AUTHOR INFORMATION

Corresponding Authors

*E-mail: jorge.castillo@uatx.mx.
*E-mail: manero@unam.mx.

ORCID

J. Castillo-Tejas: 0000-0002-2832-3499

Notes

The authors declare no competing financial interest.

ACKNOWLEDGMENTS

We acknowledge the financial support from CONACYT (project 235880) and PRODEP (project PROMEP/103.5/12/2116).

REFERENCES

(1) Dhont, J. K. G.; Briels, W. J. *Rheol. Acta* **2008**, *47*, 257−281.
(2) Hu, Y. T.; Lips, A. *J. Rheol.* **2005**, *49*, 1001−1027.
(3) Miller, E.; Rothstein, J. P. *J. Non-Newtonian Fluid Mech.* **2007**, *143*, 22−37.
(4) Boukany, P. E.; Wang, S.-Q. *Macromolecules* **2008**, *41*, 1455−1464.
(5) Callaghan, P. T. *Rheol. Acta* **2008**, *47*, 243−255.
(6) Bautista, F.; Fernández, V. V. A; Macías, E. R.; Pérez-López, J. H.; Escalante, J. I.; Puig, J. E.; Manero, O. *J. Non-Newtonian Fluid Mech.* **2012**, *177−178*, 89−96.
(7) Berret, J.-F.; Séréro, Y. *Phys. Rev. Lett.* **2001**, *87*, 048303.
(8) Sprakel, J.; Spruijt, E.; Cohen Stuart, M. A.; Besseling, N. A. M.; Lettinga, M. P.; van der Gucht, J. *Soft Matter* **2008**, *4*, 1696−1705.
(9) Marrucci, G.; Grizzuti, N. *J. Rheol.* **1983**, *27*, 433−450.
(10) Doi, M.; Edwards, S. F. *J. Chem. Soc., Faraday Trans. 2* **1979**, *75*, 38−54.
(11) Mohagheghi, M.; Khomami, B. *J. Rheol.* **2016**, *60*, 861−872.
(12) Mohagheghi, M.; Khomami, B. *ACS Macro Lett.* **2015**, *4*, 684−688.
(13) Cao, J.; Likhtman, A. E. *Phys. Rev. Lett.* **2012**, *108*, 028302.
(14) Kremer, K.; Grest, G. *J. Chem. Phys.* **1990**, *92*, 5057−5086.
(15) Castillo-Tejas, J.; Castrejón-González, O.; Carro, S.; González-Coronel, V.; Alvarado, J. F. J.; Manero, O. *Colloids Surf., A* **2016**, *491*, 37−49.
(16) Khalatur, P. G.; Khokhlov, A. R.; Mologin, D. A. *J. Chem. Phys.* **1998**, *109*, 9602−9613.
(17) Evans, D.; Morriss, G. *Statistical Mechanics of non-equilibrium liquids*, 2nd ed.; ANU E Press: Australia, 2007; p 133.
(18) Lees, A. W.; Edwards, S. F. *J. Phys. C: Solid State Phys.* **1972**, *5*, 1921−1929.
(19) Nosé, S. *J. Chem. Phys.* **1984**, *81*, 511−519.

DOI: 10.1021/acsmacrolett.6b00906
ACS Macro Lett. 2017, 6, 190−193